




Article

Synthesis and Fabrication of $\text{Co}_{1-x}\text{Ni}_x\text{Cr}_2\text{O}_4$ Chromate Nanoparticles and the Effect of Ni Concentration on Their Bandgap, Structure, and Optical Properties

Muhammad Saeed ^{1,2}, Malika Rani ³, Kiran Batool ³, Hafiza Batool ³, Aisha Younus ⁴, Sikander Azam ^{5,*} , Arshad Mehmood ⁶, Bakhtiarul Haq ⁷, Thamraa Alshahrani ^{8,*}, Ghafar Ali ⁹ and Muhammad Maqbool ^{10,*}

- ¹ State Key Laboratory of Nuclear Resour. and Environment, East China University of Technology, Nanchang 330013, China; sunrise28365@gmail.com
- ² Department of Physics, East China University of Technology, Nanchang 330013, China
- ³ Department of Physics, The Women University Multan, Multan 66000, Pakistan; mbt46037@gmail.com (M.R.); khantahirzeb@gmail.com (K.B.); wazirm495@gmail.com (H.B.)
- ⁴ Department of Physics, University of Agriculture Faisalabad, Punjab 38000, Pakistan; mhm35226@gmail.com
- ⁵ Department of Physics, RIPHAH International University I-14 Campus Islamabad, Territory 46000, Pakistan
- ⁶ National Institute of Laser & Optronics, Islamabad 45650, Pakistan; maqbool_m@yahoo.com
- ⁷ Advanced Functional Materials & Optoelectronics Laboratory (AFMOL), King Khalid University, Abha 61421, Saudi Arabia; hunainmaqbool2007@gmail.com
- ⁸ Department of Physics, College of Science, Princess Nourah Bint Abdulrahman University, Riyadh 11671, Saudi Arabia
- ⁹ Nanomaterials Research Group, Physics Division, PINSTECH, Islamabad 44000, Pakistan; iftikharahmad2021@yahoo.com
- ¹⁰ Department of Clinical & Diagnostic Sciences, Health Physics Program, the University of Alabama at Birmingham, Birmingham, AL 35294, USA
- * Correspondence: Sikander.physicst@gmail.com (S.A.); thmalshahrani@pnu.edu.sa (T.A.); mmaqbool@uab.edu (M.M.)



Citation: Saeed, M.; Rani, M.; Batool, K.; Batool, H.; Younus, A.; Azam, S.; Mehmood, A.; Haq, B.; Alshahrani, T.; Ali, G.; et al. Synthesis and Fabrication of $\text{Co}_{1-x}\text{Ni}_x\text{Cr}_2\text{O}_4$ Chromate Nanoparticles and the Effect of Ni Concentration on Their Bandgap, Structure, and Optical Properties. *J. Compos. Sci.* **2021**, *5*, 247. <https://doi.org/10.3390/jcs5090247>

Academic Editors:
Francesco Tornabene and
Thanasis Triantafyllou

Received: 24 July 2021
Accepted: 10 September 2021
Published: 14 September 2021

Publisher's Note: MDPI stays neutral with regard to jurisdictional claims in published maps and institutional affiliations.



Copyright: © 2021 by the authors. Licensee MDPI, Basel, Switzerland. This article is an open access article distributed under the terms and conditions of the Creative Commons Attribution (CC BY) license (<https://creativecommons.org/licenses/by/4.0/>).

Abstract: In the present work, cobalt-chromite-based pigment $\text{Co}_{1-x}\text{Ni}_x\text{Cr}_2\text{O}_4$ chromate powder and nanoparticles with various transition metal concentrations ($x = 0.2, 0.4, 0.6,$ and 0.8) were manufactured by applying aqueous synthesis approaches and sol-gel synthesis routes. XRD analysis of the powder shows that all samples formulated by the sol-gel method were crystalline with a spinel structure. Chromites show green color with a higher nickel concentration, while Co-substituent shows blackish pigments. Samples were annealed at distinct temperatures ranging from $600\text{ }^\circ\text{C}$ to $750\text{ }^\circ\text{C}$. The nanoparticles obtained were characterized by X-ray diffraction (XRD), scanning electron microscopy (SEM), Raman spectroscopy (RS), photoluminescence (PL), and energy-dispersive X-ray spectroscopy (EDS). The particle size of the parent compound (CoCr_2O_4) ranges from 100 nm to 500 nm , as measured by SEM. The tendency of particles to form aggregates with increasing annealing temperature was observed. These compounds may be successfully used as an effective doped nickel-cobalt ceramic pigment.

Keywords: synthesis; sol-gel process; cobalt chromite powder; XRD; photoluminescence

1. Introduction

Nanoparticles (NPs) are made up of a large number of atoms or molecules bonded with each other with a total size varying from 1 nm to around 100 nm . Due to their very small sizes, NPs possess an extraordinarily high surface-area-to-volume ratio, which changes their physical-chemical properties compared to their macroscale counterparts. Due to their unique structural, magnetic, mechanical, and electrical properties, NPs are used in a wide range of applications including biosensing, drug delivery, bioimaging, catalysis, nanomanufacturing, lubrication, electronics, textile manufacturing, and water treatment systems [1–3].

Metallic and non-metal powder and nanoparticles have been gaining attraction due to their unique applications in the environmental, biomedical, optical, and electronic industries [1,2]. Metal oxides nanoparticles are among the widest used manufactured nanomaterials because of their unique properties [3]. The properties that make the nanophase structures indispensable tools in modern nanotechnology are their various nonlinear optical properties, higher ductility at elevated temperatures than coarse-grained ceramics, cold welding properties, superparamagnetic behavior, and unique catalytic, sensitivity, and selective activity. For example, the melting point of the nanosized material is lower than that of a bulk material with the same composition [4]. At the same time, nanoparticles exhibit unusual adsorptive properties and fast diffusivities, and they are not stable in critical conditions [5].

Nanoparticles of metal oxides and their mixtures have been used as ceramic pigments. Pigments have been in demand for several reasons, including their chemical and thermal stability, hiding and tinting power, and particle size. Mixed metal oxides with general spinel formula AB_2O_4 are characterized for high thermal and chemical stability and mechanical resistance [6,7]. Spinel structure has two types: one is known as normal spinel, which is characterized by A^{+2} cations occupying the tetrahedral position, and the other is characterized by B^{+3} cations occupying the octahedral structure. The subordinate possible structure is inverse spinel, which is also characterized by A^{+2} occupying one half of the tetrahedral site and B^{+3} another half of the octahedral position and all tetrahedral coordination positions [8]. Inverse spinel structure can be affected by temperature and pressure during its synthesis [9].

$CoCr_2O_4$ are normal ferromagnetic spinel with Co^{+2} ions occupying the tetrahedral A sites, and the octahedral B sites occupied by Cr^{+3} ions [9]. The compound system undergoes ferromagnetism below ferromagnetic curie temperature of $T_c = 94$ K [10]. The magnetic tangled phase diagram is obtained by the interaction of Co^{+2} and Cr^{+3} [11]. Under the spiral ordering at $T_s = 26$ K temperature, the system is multiferroic [12]. The phase transition present occurs at the lock-in transition temperature $T_l = 15$ K [13]. Nanoparticles of $CoCr_2O_4$ possess magnetic properties [9–11]. A performance like a cluster glass has been described for nanoparticles with a size of 3.1 nm [14]. Since above 310 K, $CoNiCr_2O_4$ crystallizes and attains cubic normal spinel structure, therefore, the crystal structure becomes tetragonal due to Jahn–Teller manipulation in that temperature range [15]. Lowering temperature below 65 K, the crystal structure further transforms into the orthorhombic phase [16]. Deformation within the same orthorhombic phase has been distinguished at $T = 30$ K [8]. The magnetic properties of $CoCr_2O_4$ and $CoNiCr_2O_4$ are different for Ni-doped $CoCr_2O_4$. The co-precipitation method is used to synthesize particles of standard size 80–100 nm, which are described in [17]. The property of magnetization of an applied magnetic field displays a thin characteristic measured for $Co_{0.5}Ni_{0.5}Cr_2O_4$ nanoparticles developed through the sol–gel process at $T = 10$ K, which is missing in $CoNiCr_2O_4$ and $CoCr_2O_4$ [18].

In our present work, we have synthesized cobalt-doped nickel chromite by the sol–gel method, which is easy to use and environmentally friendly. We also report that the sol–gel process needs low temperature and less calcination to achieve the desired product [19]. In this work, we are comparing base compound and doped cobalt chromites with different transition metal concentrations. The concentration of Ni is increased in steps of 0.2. The composition and size of new spinel crystal is examined in this study. Structural and surface analyses of the synthesized nanoparticles are also performed using XRD, SEM, EDS, and Raman spectroscopy. Photoluminescence is an important phenomenon that provides information about light emission from various materials and their applications in optical, photonic, and microelectronic devices and display technologies [20–23]. Photoluminescence of the $CoNiCr_2O_4$ nanoparticles is performed to investigate the suitability of these compounds and nanoparticles in optical and photonic applications.

2. Materials and Methods

For synthesis of CoCr_2O_4 , Ni doped in cobalt chromate to form nickel chromate, we used nickel nitrate, cobalt nitrate, and chromium nitrate, with 100 mL distilled water and 1,2 ethanediol added to the solution (as a complex agent). First, 100 mL purified water was taken in a beaker then nickel nitrates, cobalt, and chromium were added to it. The beaker was then placed on a hot plate with a stirrer and heated up to a temperature range between 60 and 65 °C. We waited until the solution became homogenous, and then 1,2 ethanediol was added to the reaction solution to form a gel. By continuously heating and maintaining the same temperature for 4 h, a dark green gel was obtained. The gel was then kept in a DHG-9202 oven (Jiangsu Jinyi Instrument Technology Company Limited, Jintan City, Changzhou, Jiangsu, China) at 1050 °C for 10 h to dry. After complete drying, a green-colored powder was obtained. To obtain it in a fine form of powder or nanoparticles, a grinder and agate motor was used, in which the sample was ground. VULCAN-D550 furnace was used to sinter the powder of CoCr_2O_4 and $\text{Co}_{1-x}\text{Ni}_x\text{Cr}_2\text{O}_4$ at 7000 °C for 3 h to obtain greenish-colored nanoparticles. Figure 1 shows the flow chart of manufacturing nanoparticles.

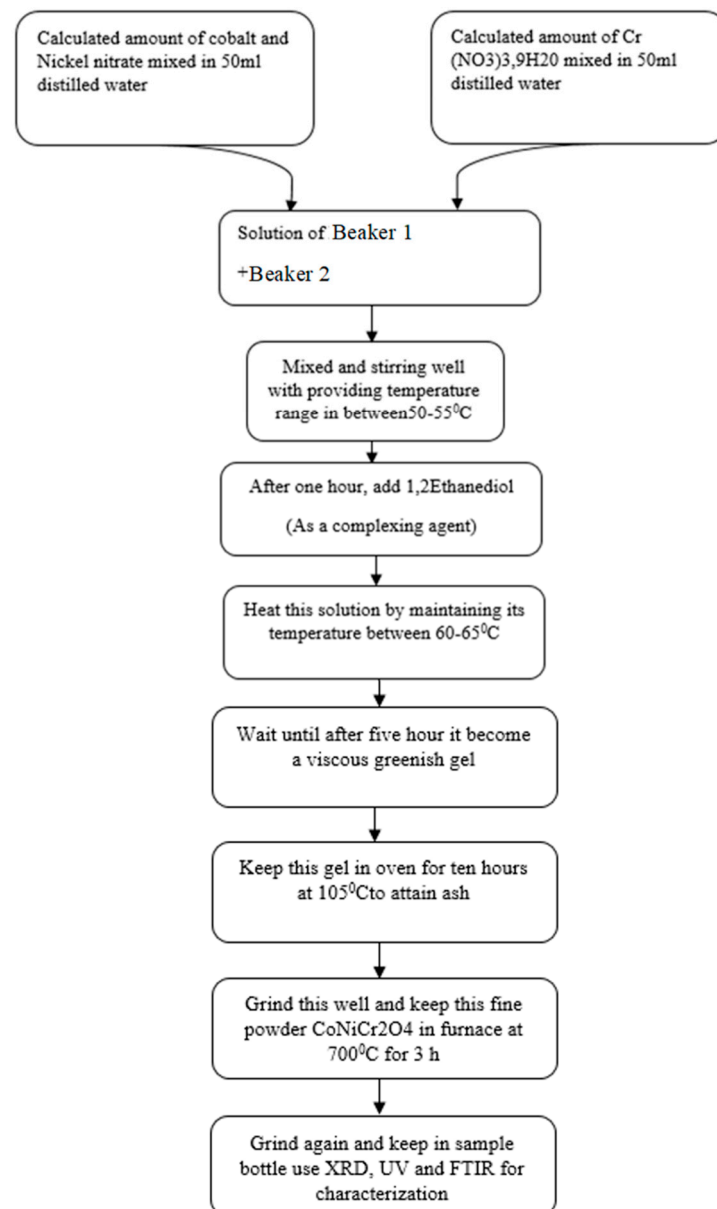


Figure 1. Schematic flowchart of manufacturing CoCr_2O_4 , $\text{CoNiCr}_2\text{O}_4$ nanoparticle.

3. Results and Discussion

3.1. XRD Analysis

Information on the phase and crystal structure of cobalt chromite is obtained through the X-ray diffraction technique. X-ray Cu-K α radiation of wavelength 1.5418 Å was used to produce the diffraction pattern. The range of angle 2θ of the XRD pattern ranges from 15° to 60°. The XRD pattern of cobalt chromite is shown in Figure 2. A single phase of cobalt chromite is obtained at a calcination temperature of 700 °C. XRD peaks corresponding to 700 °C were obtained at 15.5°, 30.5°, 35.5°, 40.5°, 45°, 50°, and 55.5°. A high pure cubic structure of cobalt chromite is synthesized through this process. Single 124 phase of cobalt chromite is obtained with reference code COD REV218120 2019.09 at 700 °C temperature. XRD analysis of cobalt chromite shows that the lattice parameters a and c range from 8.328 to 8.412 Å. Grainsize of 1.541874 Å for cobalt chromite is obtained from XRD peaks.

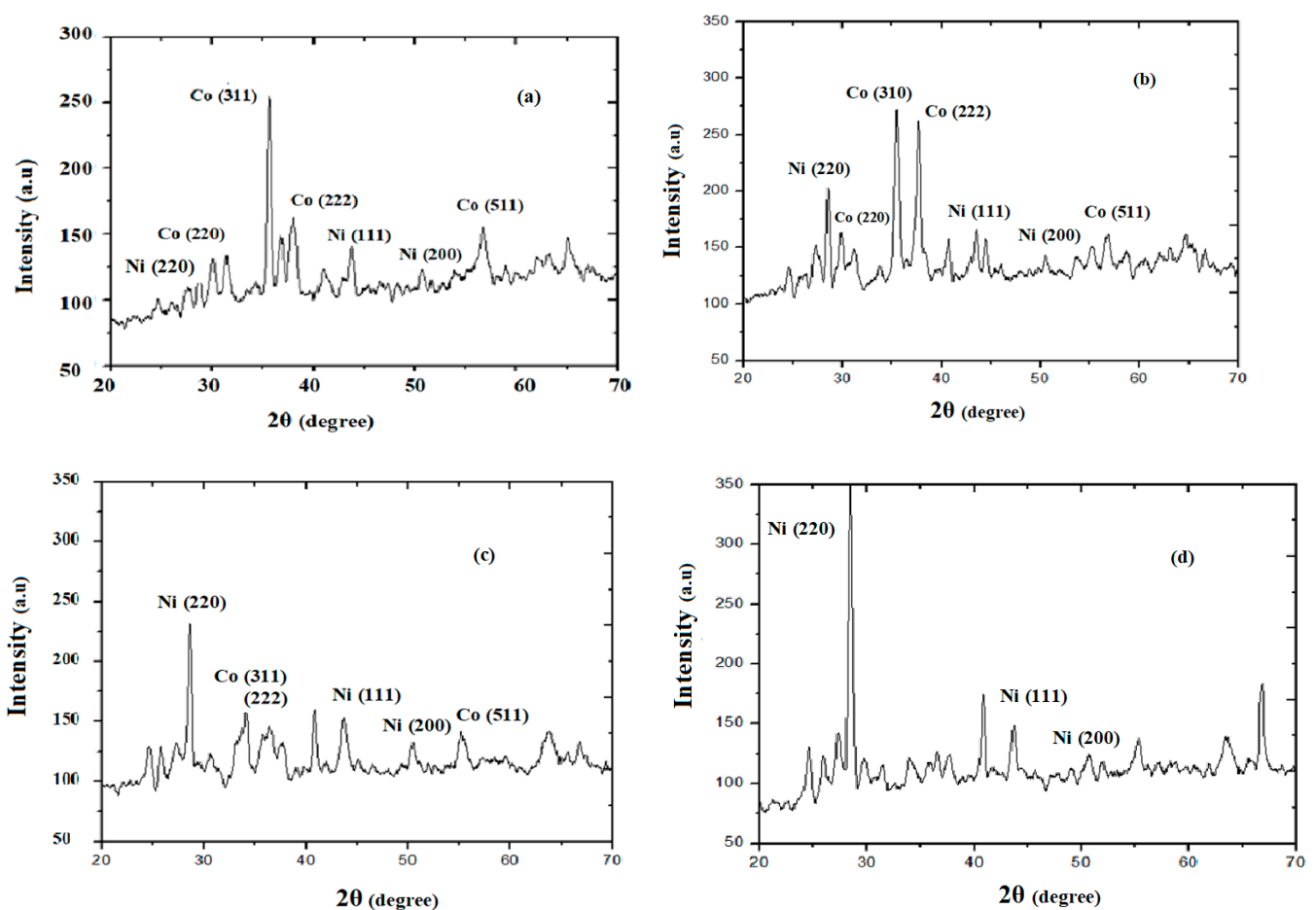


Figure 2. XRD pattern of CoCr₂O₄ and Co_{1-x}Ni_xCr₂O₄: (a) $x = 0.2$, (b) $x = 0.4$, (c) $x = 0.6$, and (d) $x = 0.8$.

The X-ray diffraction pattern of Ni powders substituted with Co_{1-x}Ni_xCr₂O₄ depending on calcination temperature was attained by sol-gel process. Analysis of phase composition shows the sample with a high substitution rate at $x = 0.2, 0.4, 0.6$, and 0.8 , with no single-phase compound for all temperatures. X-ray diffraction shows that the substitution of cobalt from nickel chromite proceeds by the steady transformation of cubic CoCr₂O₄ crystalline phase into cubic CoNiCr₂O₄ spinel state. In the pigmentary field, the main objective is to get the proper parameters of pigments used in industry [14].

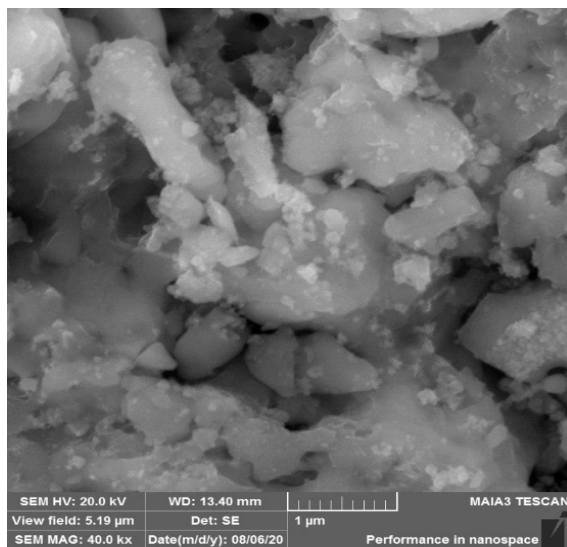
The estimated size of cobalt chromite crystallites is 48.9 nm, obtained from heat treatment at 700 °C. For the nanoparticles, Co_{1-x}Ni_xCr₂O₄ crystallite size varied with heat treatment at 700 °C in the 39.5–44.5 nm range. The size of crystallite increases by less than 10 nm for all temperatures in this range.

The average linear crystallite size can be calculated using Bragg's equation, $n\lambda = 2d \sin \theta$, where n is an integer, θ is the angle between the incident and scattered ray, d is the inter-spacing distance, and λ is the wavelength associated with the particle. Crystal size D of a particle can also be calculated by using Scherrer's equation, $D = K\lambda/\beta \cos \theta$, where K is the crystalline shape constant.

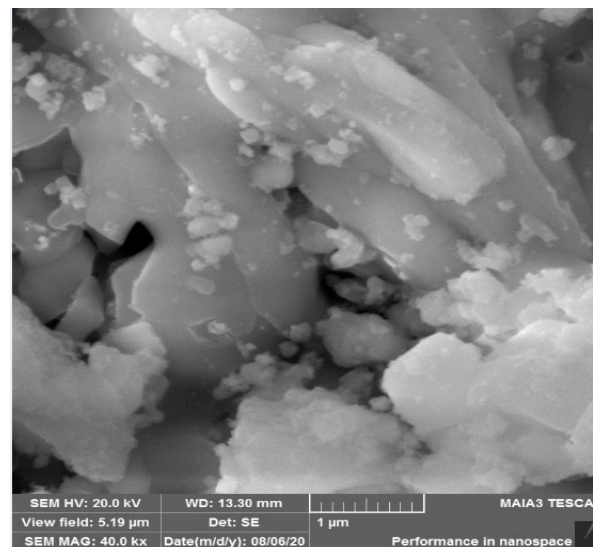
XRD results show that the powder form nanoparticles achieved from the sol-gel process is still heterogenous but more homogenous than that obtained by other techniques. However, phase composition is identical to the parent compound; yet, the morphology of synthesized pigments differed significantly.

3.2. SEM Analysis

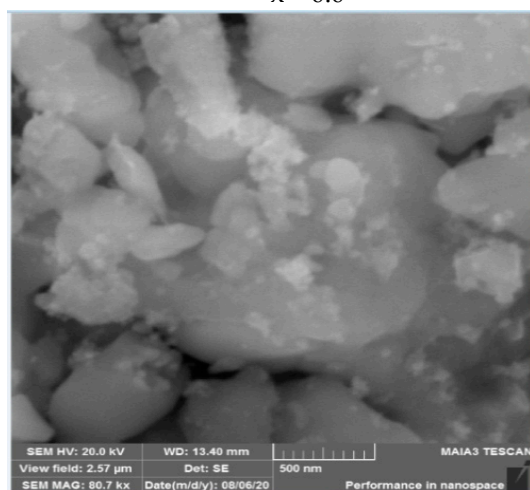
The morphology of samples obtained by methods of synthesis is quite different than others. SEM micrographs of sol-gel-obtained samples of $\text{CoNiCr}_2\text{O}_4$ heated at 700°C and CoCr_2O_4 have different morphological features, as shown in Figure 3. Very small spherical nanosized particles of CoCr_2O_4 were synthesized, showing a high degree of agglomeration.



$x = 0.0$



$x = 0.4$



$x = 0.6$

Figure 3. SEM images of $\text{Cu}_{1-x}\text{Ni}_x\text{Cr}_2\text{O}_4$ ($x = 0.0, 0.4,$ and 0.6).

Different shaped and bigger sized (150–200 nm) particles of $\text{CoNiCr}_2\text{O}_4$ were obtained in synthesis. The surface morphology of doped cobalt chromite is very similar to cobalt

chromite. The obtained powder largely consists of irregular, sub-micron shape particles of size 110 nm–500 nm, which resulted in a few large agglomerates with a porous microstructure.

3.3. Raman Spectroscopy

Raman spectroscopy of nickel doped in cobalt chromite, with the concentrations of nickel as 0.2, 0.4, and 0.6, was performed. Raman spectroscopy graph is plotted between intensity in (a.u) and Raman shift in cm^{-1} ranging from 1000 to 1600 cm^{-1} with a spacing of 100 cm^{-1} , and peaks are obtained at 1440 cm^{-1} and 1540 cm^{-1} , which shows the purity of the sample. No impurity peak is observed because of Raman spectroscopy. The Raman spectroscopy graph of nickel-doped cobalt chromite is shown in Figure 4.

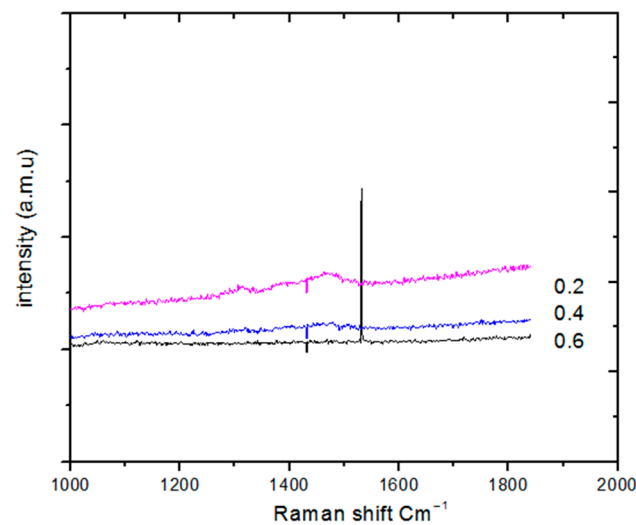


Figure 4. Raman spectroscopy of doped cobalt chromites $\text{Co}_{1-x}\text{Ni}_x\text{Cr}_2\text{O}_4$.

3.4. EDS Spectroscopy

Energy-dispersive spectroscopy (EDS), which is also called energy-dispersive analysis, was performed for the synthesized samples. Figure 5 shows results from EDS spectroscopy of our samples. The figure clearly shows that a single phase of copper chromite has formed. No extra impurity peak appeared in the EDS spectrum. We have obtained a single phase of copper chromite.

3.5. Photoluminescence

Figure 6 shows the photoluminescence spectrum of nanoparticles. An excitation wavelength of 347 nm was used in this work at room temperature. It is important to monitor the physical properties of nanoparticles that change with variations in their dimensions on the nanometer scale, known as the quantum size effect. For example, quantum confinement increases the required energy bandgap of CoCr_2O_4 observed in photoluminescence. The recombination of the surface state is also evident from photoluminescence. The spectrum exhibits two emission peaks. One is located at 380 nm in the UV region, corresponding to near bandgap excitonic emission. The second peak is positioned around 530 nm, which can be attributed to the occupancy of independently ionized Co vacancies. Furthermore, the narrow size distribution of nanoparticles in luminescence, with a full width and half maximum (FWHM) of only a few nanometers, is reported by spectrum.

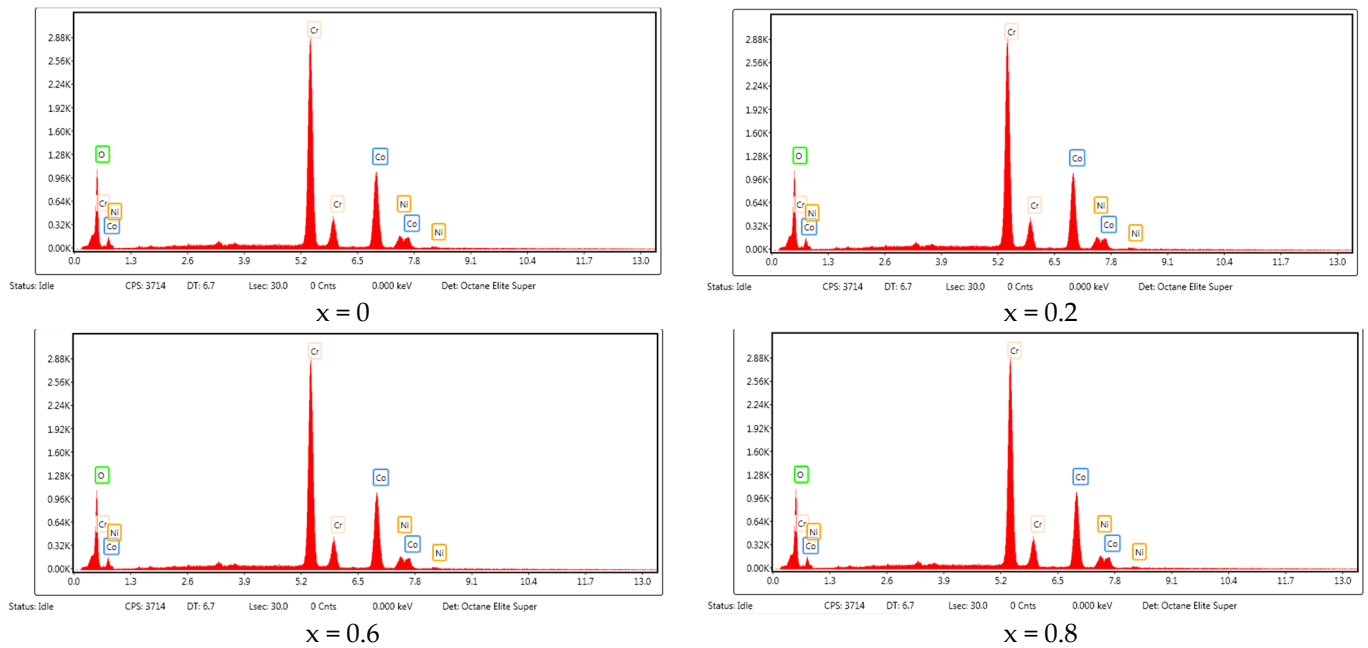


Figure 5. EDS results of $\text{Co}_{1-x}\text{Ni}_x\text{Cr}_2\text{O}_4$ ($x = 0.2, 0.4, 0.6, 0.8$).

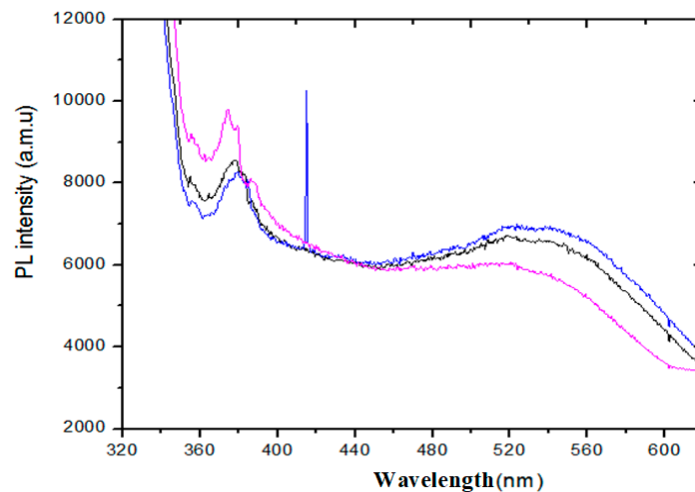


Figure 6. Photoluminescence spectra of doped $\text{Co}_{1-x}\text{Ni}_x\text{Cr}_2\text{O}_4$.

To further shed light on these compounds, the compounds prepared by the sol–gel synthesis route were formed with higher pronounced crystallinity. The morphological features of the samples derived by both synthesis methods are quite different. Moreover, the size and shape of chromite particles depend not only on the synthesis method used, but also on the nature of the octahedral cation A^{+2} . The origin of cation A^{+2} in the spinel structure displayed the tendency to produce pigments of numerous hues. The increase of Ni^{+2} content leads to a warm black color. The Co^{+2} enrichment in tetrahedral ligand field gives a variety of green shades, from bluish-green to yellowish-green. Only Cu-doped pigments exhibited fewer different hues and were dark, nearly black. Nonetheless, there are no main differences in the colors between pigments produced by the sol–gel synthesis methods.

4. Conclusions

Two aqueous sol–gel and sonochemical synthesis methods were successfully employed for the preparation of the chromite spinels $\text{Co}_{1-x}\text{Ni}_x\text{Cr}_2\text{O}_4$ ($x = 0–1$ with a step of 0.2). The single-phase cobalt-chromium spinel CoCr_2O_4 and nickel-doped chromates were

synthesized irrespective of the calcination temperatures (600–700 °C). However, the phase compositions of Ni-substituted chromates were found to be dependent on the annealing temperature. At higher substitution ratios of 0.6 and 1, these samples were mixtures of spinel-type and simple oxide crystalline phases. When the concentration of the Ni dopant is increased, the Co peak is suppressed. The work is important in its applications for optical devices and enhanced photocatalytic applications.

Author Contributions: M.S. (research investigations), M.R. (project administration), K.B. (conceptualization), H.B. (data validation), A.Y. (software and data analysis), S.A. (methodology and writing original text), A.M. (art work and figures), B.H. (revisions and validation), T.A. (funding and project development), G.A. (data analysis and validation), M.M. (supervision and editing draft). All authors have read and agreed to the published version of the manuscript.

Funding: This research was funded by Princess Nourah Bint Abdulrahman University internal grant.

Data Availability Statement: The data presented in this study are available on request from the corresponding author.

Acknowledgments: The authors extend their sincere appreciation to the Deanship of Scientific Research at Princess Nourah Bint Abdulrahman University, for the support through the Fast-track Research Funding Program.

Conflicts of Interest: The authors declare no conflict of interest.

References

1. Kaur, A.; Gupta, U. A review on applications of nanoparticles for the preconcentration of environmental pollutants. *J. Mater. Chem.* **2009**, *19*, 8279–8289. [[CrossRef](#)]
2. Han, X.; Xu, K.; Taratula, O.; Farsad, K. Applications of nanoparticles in biomedical imaging. *Nanoscale* **2019**, *11*, 799–819. [[CrossRef](#)] [[PubMed](#)]
3. Chavali, M.S.; Nikolova, M.P. Metal oxide nanoparticles and their applications in nanotechnology. *SN Appl. Sci.* **2019**, *1*, 607. [[CrossRef](#)]
4. Castro Alarcon, N.; Herrera Arizmendi, J.L.; Luis Alberto, M.C.; Guzman Guzman, I.P.; Perez Centeno, A.; Santana Aranda, M.A. Antibacterial activity of nanoparticles of titanium dioxide, intrinsic and doped with indium and iron. *Microbiol. Res. Int.* **2016**, *4*, 55–62.
5. Bindhu, M.; Umadevi, M.; Micheal, M.K.; Arasu, M.V.; Al-Dhabi, N.A. Structural, morphological and optical properties of MgO nanoparticles for antibacterial applications. *Mater. Lett.* **2016**, *166*, 19–22. [[CrossRef](#)]
6. De Souza, L.K.C.; Zamian, J.R.; da Rocha Filho, G.N.; Soledade, L.E.; dos Santos, I.M.; Souza, A.G.; Scheller, T.; Angélica, R.S.; da Costa, C.E.F. Blue pigments based on $\text{Co}_x\text{Zn}_{1-x}\text{Al}_2\text{O}_4$ spinels synthesized by the polymeric precursor method. *Dyes Pigments* **2009**, *81*, 187–192. [[CrossRef](#)]
7. Lorenzi, G.; Baldi, G.; Di Benedetto, F.; Faso, V.; Lattanzi, P.; Romanelli, M. Spectroscopic study of a Ni-bearing gahnite pigment. *J. Ceram. Soc.* **2006**, *26*, 317–321. [[CrossRef](#)]
8. Sickafus, K.E.; Wills, J.M.; Grimes, N.W. Structure of spinel. *J. Am. Ceram. Soc.* **1999**, *82*, 3279–3292. [[CrossRef](#)]
9. Wang, Z.; Lazor, P.; Saxena, S.; Artioli, G. High-Pressure Raman Spectroscopic Study of Spinel (ZnCr_2O_4). *J. Solid State Chem.* **2002**, *165*, 165–170. [[CrossRef](#)]
10. Torgashev, V.I.; Prokhorov, A.; Komandin, G.; Zhukova, E.; Anzin, V.B.; Talanov, V.M.; Rabkin, L.M.; Bush, A.A.; Dressel, M.; Gorshunov, B.P. Magnetic and dielectric response of cobalt-chromium spinel CoCr_2O_4 in the terahertz frequency range. *Phys. Solid State* **2012**, *54*, 350–359. [[CrossRef](#)]
11. Lawes, G.; Melot, B.; Page, K.; Ederer, C.; Hayward, M.A.; Proffen, T.; Seshadri, R. Dielectric anomalies and spiral magnetic order in CoCr_2O_4 . *Phys. Rev. B* **2006**, *74*, 024413. [[CrossRef](#)]
12. Tsurkan, V.; Zherlitsyn, S.; Yasin, S.; Felea, V.; Skourski, Y.; Deisenhofer, J.; Krug von Nidda, H.-A.; Wosnitza, J.; Loidl, A. Unconventional magnetostructural transition in CoCr_2O_4 at high magnetic fields. *Phys. Rev. Lett.* **2013**, *110*, 115502. [[CrossRef](#)] [[PubMed](#)]
13. Yamasaki, Y.; Miyasaka, S.Y.; Kaneko, Y.; He, J.-P.; Arima, T.; Tokura, Y. Magnetic Reversal of the Ferroelectric Polarization in a Multiferroic Spinel Oxide. *Phys. Rev. Lett.* **2006**, *96*, 207204. [[CrossRef](#)] [[PubMed](#)]
14. Kumar, L.; Mohanty, P.; Shripathi, T.; Rath, C. Appearance of superparamagnetic phase below Curie temperature in cobalt chromite. *Nanosci. Nanotechnol. Lett.* **2009**, *1*, 199–2002. [[CrossRef](#)]
15. Zakunta, D.; Vlcek, J.; Fitl, P.; Nemokovski, K.; Honecker, D.; Niznansky, D.; Disch, S. Noncollinear magnetism in nanosized cobalt chromite. *Phys. Rev. B* **2019**, *98*, 064407.
16. Suchomel, M.R.; Shoemaker, D.P.; Ribaud, L.; Kemei, M.C.; Seshadri, R. Spin-induced symmetry breaking in orbitally ordered NiCr_2O_4 and CuCr_2O_4 . *Phys. Rev. B* **2012**, *86*, 054406. [[CrossRef](#)]

17. Mohanty, P.; Sheppard, C.J.; Prinsloo, A.R.E.; Roos, W.D.; Olivi, L.; Aquilanti, G. Effect of cobalt substitution on the magnetic properties of nickel chromite. *J. Magn. Magn. Mater.* **2018**, *451*, 20–28. [[CrossRef](#)]
18. Mohanty, P.; Prinsloo, A.R.E.; Doyle, B.P.; Carleschi, E.; Sheppard, C.J. Structural and magnetic properties of $(\text{Co}_{1-x}\text{Ni}_x)\text{Cr}_2\text{O}_4$ ($x = 0.5, 0.25$) nanoparticles. *AIP Adv.* **2018**, *8*, 056424. [[CrossRef](#)]
19. Opuhovic, O.; Kreiza, G.; Servaitiene, J.; Kazlauskas, K.; Beganskiene, A.; Kareiva, A. Sol-Gel synthesis, characterization and application of selected sub-micro sized lanthanide (Ce, Pr, Nd, Tb) ferrites. *Dyes Pigments* **2015**, *118*, 176–182. [[CrossRef](#)]
20. Maqbool, M.; Ahmad, I.; Ali, G.; Maaz, K. Energy level splitting and luminescence enhancement in AlN: Er by an external magnetic field. *Opt. Mater.* **2015**, *46*, 601–604. [[CrossRef](#)]
21. Maqbool, M.; Ali, G.; Ahmad, I.; Maaz, K. Luminescence Enhancement in Amorphous AlN: W by Direct UV Excitation through Co-Doped Gadolinium. *IEEE Photonics Technol. Lett.* **2015**, *27*, 1519–1522. [[CrossRef](#)]
22. Maqbool, M.; Main, K.; Kordesch, M. Titanium doped sputter-deposited AlN infrared whispering gallery mode microlaser on optical fibers. *Opt. Lett.* **2010**, *35*, 3637–3639.
23. Maqbool, M.; Ahmad, I.; Richardson, H.H.; Kordesch, M.E. Direct ultraviolet excitation of an amorphous AlN: Praesiodimium phosphor by co-doped Gd^{3+} Cathodoluminescence. *Appl. Phys. Lett.* **2007**, *91*, 193511. [[CrossRef](#)]